Large-scale gyrokinetic turbulence simulations: Effects of profile variation*

Scott E. Parker,† Charlson Kim, and Yang Chen
Center for Integrated Plasma Studies, Department of Physics, University of Colorado at Boulder, Boulder, Colorado 80309

(Received 16 November 1998; accepted 13 January 1999)

Two common computational domains used in gyrokinetic turbulence simulations are a local flux-tube and a global whole plasma volume. The effect of a radially varying pressure gradient is found to explain some of the qualitative differences between these two models. It is shown that a coherent purely radial mode is the result of profile variation. In addition, as profile variation is increased, there is a fairly sudden transition to much lower levels of heat flux. This may explain lower values found in past global simulations. The self-generated purely radial electrostatic potential is found to be 180° out of phase with the flux-surface-averaged ion temperature. A theoretical relation between these two quantities is derived by relating the $E\times B$ nonlinearities for ion density and temperature for purely radial modes. This relation is used to explain the various radial mode shapes. Extending these results, a possible scheme is explored to reduce the heat flux by adding a ripple to the ion temperature profile. It may be possible to achieve similar results experimentally using ion cyclotron resonance heating. Finally, simulation results show the additional stabilizing effect of equilibrium E_r shear from profile variation in the radial force balance equation. © *1999 American Institute of Physics.* [S1070-664X(99)92805-7]

I. INTRODUCTION

Gyrokinetic simulation of tokamak plasmas has reached a level of realism qualitatively different than turbulence simulations five to ten years ago.[1–4] This realism has been possible due to the development of gyrokinetics,[5,6] developments in low-noise δf methods,[7–9] and massively parallel computing.[10,11] Large-scale gyrokinetic simulations are now an accepted and important tool in our continued effort to better understand anomalous transport in magnetic fusion plasmas. There are two common computational domains. Global simulations, which model the whole tokamak cross section, are able to simulate plasmas with a minor radius as large a $200\rho_i$ (Refs. 3, 4, and 10) on current generation massively parallel supercomputers. Flux-tube simulations are able to simulate arbitrarily large tokamak plasmas and/or much higher spatial resolution, but with assumptions of locality of the turbulence.[2,12–14] This model greatly reduces the volume of the simulation domain, and, hence, the computational requirements. It does however, require imposing more assumptions which will be discussed in Sec. II.

When solving virtually any kinetic plasma problem, one is immediately faced with an enormous disparity in space–time scales.[15] Fortunately, for low-frequency magnetized plasmas, there is an analytic reduction to the Vlasov–Maxwell system, called gyrokinetics. A perturbative expansion is made in the following small quantities $\epsilon\sim\omega/\Omega_i \sim e\phi/T_e\sim \delta n/n\sim k_\parallel/k_\perp\sim\rho_i/L\sim\epsilon$, where ϵ is small and L is representative of the equilibrium gradient scale lengths. The Vlasov–Maxwell system is then averaged over the fast gyro-motion, retaining finite Larmor radius (FLR) effects. Gyrokinetic theory evolved from linear equations in the 1970s to fully nonlinear in the 1980s.[5,6,16–19] It is now well accepted that the gyrokinetic equations are a good starting point for low-frequency tokamak plasma physics.

The gyrokinetic equation is very similar to the more basic Vlasov equation. It is still a continuity equation, but in a reduced five-dimensional phase space for particle guiding centers, with the familiar form

$$\frac{\partial f}{\partial t}+\dot{\mathbf{z}}\cdot\frac{\partial f}{\partial \mathbf{z}}=0, \tag{1}$$

where $\mathbf{z}=(\mathbf{R},v_\parallel,\mu)$, $\mathbf{R}$ is the guiding center position, and $v_\parallel$ is the velocity along the magnetic field. The equation of motion for a guiding center defines $\dot{\mathbf{z}}$ and it includes gyroaveraging of field quantities. $\mu\equiv mv_\perp^2/(2B)$ is time independent.

Our approach to solving Eqs. (1) is to first write the total distribution function in terms of the equilibrium and perturbed parts $f(\mathbf{z},t)=f_0(\mathbf{z})+\delta f(\mathbf{z},t)$. $\dot{\mathbf{z}}$ is expanded into equilibrium and perturbed parts as well $\dot{\mathbf{z}}=\dot{\mathbf{z}}^0+\dot{\mathbf{z}}^1$. $f_0(\mathbf{z})$ is an equilibrium distribution which satisfies $\dot{\mathbf{z}}^0\cdot\partial_{\mathbf{z}}f_0(\mathbf{z})=0$. The equation for δf is

$$\partial_t\delta f+\dot{\mathbf{z}}\cdot\partial_{\mathbf{z}}\delta f=-\dot{\mathbf{z}}^1\cdot\partial_{\mathbf{z}}f_0. \tag{2}$$

This equation is solved by following characteristics along particle trajectories. We define the particle weights w_i as[8]

$$w_i\equiv\left.\frac{\delta f}{f}\right|_{\mathbf{z}=\mathbf{z}_i,t}. \tag{3}$$

*Paper G4TV.1 Bull. Am. Phys. Soc. **43**, 1733 (1998).
†Tutorial speaker.

The weights are evolved in time and are deposited on the grid. In contrast, conventional particle-in-cell methods deposit a unit of charge for each particle.

Only electrostatic simulations of ion-temperature-gradient-driven turbulence will be discussed in this paper. We will use full gyro-phase-averaged ion dynamics, including trapped particles and assume adiabatic electrons $\delta n_e/n_0 = e(\phi - \langle\phi\rangle)/T_e$.[14,20] The quasi-neutrality condition[6,21] in Fourier space is

$$-\rho_s^2/(\rho_i^2\lambda_D^2)[1-\Gamma_0(b)]\phi = -4\pi e(\delta\overline{n_i} - \delta n_e), \qquad (4)$$

where $\delta n = (n-n_0)/n_0$, $\delta\overline{n_i}$ is the gyro-phase-averaged ion density, $b=(k_\perp\rho_i)^2$, $\rho_s^2 \equiv T_e/T_i\rho_i^2$, $\lambda_D \equiv \sqrt{T_e/(4\pi n_0 e^2)}$, and higher-order terms have been neglected in Eq. (7). In the small b limit Eq. (4) reduces to $(\rho_s/\lambda_D)^2\nabla_\perp^2\phi = -4\pi e(\delta\overline{n_i} - \delta n_e)$. To avoid any confusion, throughout this paper $T_i = T_e$ and $\rho_i = \rho_s$.

In Sec. I, we discuss global and flux-tube models in more detail. In Sec. II, we discuss temperature and density profile variation as one of the primary differences between the two models. We also show and give a theoretical explanation for the relationship between flux-surface-averaged electrostatic potential $\langle\phi\rangle$ and the flux-surface-averaged perpendicular ion temperature $\langle T_\perp\rangle$. In Sec. IV, this relationship motivates a possible technique to reduce turbulent transport by adding a small ripple to the temperature profile. Finally, we discuss the additional stabilizing effect of equilibrium E_r shear from variation of ∇P_i in the ion radial force balance equation.

II. COMPUTATIONAL DOMAINS: GLOBAL AND FLUX-TUBE

There are two common computational domains used for toroidal gyrokinetic simulation: a global volume or whole plasma cross section, and a flux-tube volume using local plasma parameters. Annular volumes are also used,[4,22] but to a lesser extent because the volume of the hollow core is typically less than the annular volume, i.e., $r_2^2 - r_1^2 \gtrsim r_1^2$, where r_1 and r_2 are the inner and outer radii of the annulus. In many ways, global simulations are easier to implement and few approximations need to be made. On the other hand, they require an enormous amount of computer time. Plasma volumes the size of DIII-D[23] are possible, $\rho_i/a \sim 200$, but require many hours of computer time on the largest massively parallel machines available. Flux-tube simulations have the advantage that they simulate the minimal plasma volume necessary to capture the important (conventional) physics and can simulate arbitrarily large tokamak plasmas. However, many assumptions go into flux-tube simulations. Most importantly, local quantities are used that only keep first-order derivatives in modeling the equilibrium variation. In addition, it is assumed that the turbulence is decorrelated across the box in the perpendicular direction.

Global models have been used quite extensively to investigate the ion-temperature-gradient-driven (ITG) instability.[1,3,10] The global simulation discussed here uses a square cross section which is suitable for spectral solution of the field equation. The simulation coordinates used here are (x,y,ψ) and are related to the usual toroidal coordinates (r,θ,ψ) through $x = r\cos\theta$ and $y = r\sin\theta$. This is simply the usual cylindrical coordinates (R,Z,ψ). Using these coordinates, assuming $(k_\parallel/k_\perp)(B_\theta/B_\psi) \ll 1$, where B_θ and B_ψ are the poloidal and toroidal components of $\mathbf{B}$ with $\mathbf{k}_\perp = (k_x\rho_s, k_y\rho_s)$, Eq. (4) is solved with higher-order terms neglected. Here ρ_s is assumed constant in Eq. (4). For the radial boundary condition we set $\overline{n_i}$ to zero for $r \geqslant (a - 4\rho_s)$ within the square cross section. The magnetic field is fixed and specified by $B_\psi = B_0R_0/R$, $B_\theta = rB_\psi/(R_0q(r))$, and $q(r) = q_0 + \Delta q(r/a)^2$. Initial equilibrium density and temperature profiles are used such that $L_n^{-1} \equiv |\nabla n|/n$ and $L_T^{-1} \equiv |\nabla T|/T$ have a radial variation proportional to $\mathrm{sech}^2[(r - r_0)/w]$, where r_0 and w as well as the peak normalized gradients $L_n^{-1}(r_0)$ and $L_T^{-1}(r_0)$ are all specified parameters.

It will be useful to define a base set of parameters that will be referred to later in the paper when discussing the results: 34 million particles, a $256\times256\times128$ grid in (x,y,ψ), with a perpendicular grid cell size $\Delta x = \Delta y = 1.25\rho_s$, and a time step of $\Delta t c_s/L_T = 0.16$. The physical parameters are $R_0/L_T(r_0) = 6.9$, $R/L_n(r_0) = 2.2$, $T_i = T_e$, $a = 160\rho_s$, and $R_0 = 445\rho_s$, $q_0 = 0.85$, $\Delta q = 2.2$, $w = 40\rho_s$, $r_0 = \frac{1}{2}a$ is the location of the maximum temperature and density gradients (see above), $q(r_0) = 1.4$, $\hat{s} \equiv (r/q)(dq/dr) = 0.78$ at r_0. We will call these the ''DIII-D base case'' parameters which is representative of a typical H-mode plasma (D-IIID Shot 81499), but assume a circular zero-beta large aspect ratio magnetohydrodynamic (MHD) equilibrium, no impurities, adiabatic electrons, and no fast ions. These parameters were used by the ''Cyclone Team,'' a Department of Energy initiative to study the physics basis of transport models used for the prediction of the International Thermonuclear Experimental Reactor.[24]

Next, we discuss the flux-tube model. The simulation domain is a magnetic flux tube and contains the minimum plasma volume necessary to model high-n drift-type microinstabilities by utilizing the alignment of the long twisted eddies, i.e., $k_\parallel \ll k_\perp$.[14,25] Figure 1 shows the flux-tube computational domain for the D-IIID base case parameters. The bottom figure using a $L_x\times L_y = 128\rho_s\times128\rho_s$ grid pushes the limits of the ''local'' flux-tube model. The field-line-following coordinates used in this simulation are[14]

$$x = r - r_0, \quad y = \frac{r_0}{q_0}(q(r)\theta - \psi), \quad z = Rq_0\theta, \qquad (5)$$

where r is the minor radius, θ is the poloidal angle, ψ is the toroidal angle, q is the safety factor, $q_0 = q(r_0)$, and $R = R_0$ is the major radius. The width of the box in the radial direction is assumed small compared to r_0, dq/dr is assumed constant. A zero β unshifted circular magnetic equilibrium and small r_0/R are also assumed. The domain is rectilinear in the field-line-following coordinates and is taken to be periodic in x and y. At the ends of the box $z = \pm Rq_0\pi$ periodicity in θ and ψ is enforced.[14] These boundary conditions may be justified if the box size is larger than the correlation length in the perpendicular directions. The particle equations of motion used in the simulation are obtained by transforming Hamiltonian guiding center equations,[26] keeping terms first

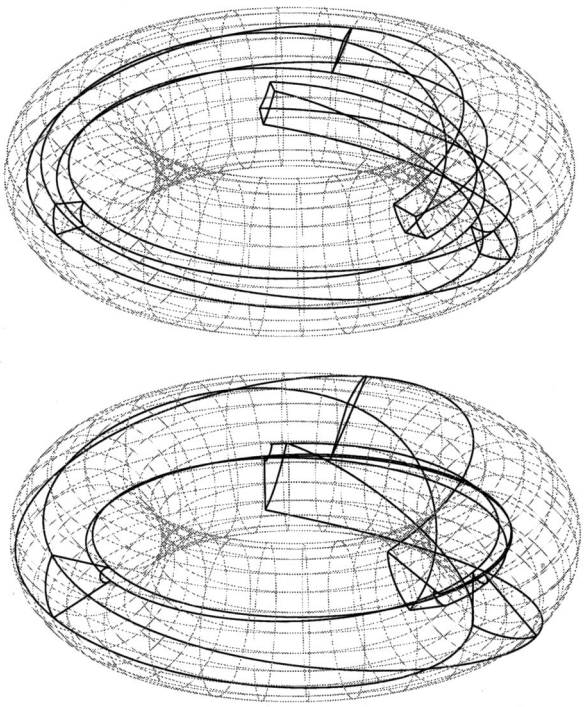

FIG. 1. Geometry of the flux-tube computational domain with the D-IIID base case parameters. The torus shown is the full plasma size and the flux-tube domain has $L_x \times L_y = 64\rho_s \times 64\rho_s$ (top) and $L_x \times L_y = 128\rho_s \times 128\rho_s$ (bottom).

order in r/R, to the field-line-following coordinates. Details of the gyrokinetic formalism in magnetic coordinates can be found in Ref. 18. This twisted nonorthogonal coordinate system has the following ''nice'' gradient operators:

$$\hat{\mathbf{b}} \cdot \nabla f = \frac{\partial f}{\partial z}, \tag{6}$$

$$(\hat{b} \times \nabla \phi) \cdot \nabla f = \frac{\partial \phi}{\partial y}\frac{\partial f}{\partial x} - \frac{\partial \phi}{\partial x}\frac{\partial f}{\partial y}, \tag{7}$$

$$\nabla_\perp^2 \phi = \frac{\partial^2 \phi}{\partial x^2} + (1 + s^2 z^2)\frac{\partial^2 \phi}{\partial y^2} + 2sz\frac{\partial^2 \phi}{\partial x \partial y}, \tag{8}$$

to leading order, where $s = 1/L_s = r_0 q'/Rq^2$. The variation of the ρ_i along the magnetic field line can be taken into account in quasi-neutrality equation, Eq. (4), using $\rho_i^2 = 1 + 2(r_0/R)\cos\theta$, so that

$$k_\perp^2 \rho_i^2 = [k_x^2 + (1 + s^2 z^2)k_y^2 + 2szk_x k_y][1 + 2(r_0/R)\cos\theta]. \tag{9}$$

The DIII-D base case parameters are: 8 particles per cell, $128 \times 128 \times 32$ grid, with $\Delta x = \Delta y = \rho_s$, and a time step of $\Delta t c_s/L_T = 0.037$. The physical parameters are $R/L_T = 6.9$, $R/L_n = 2.2$, $T_e/T_i = 1$, $r/R = 0.18$, $q = 1.4$, $\hat{s} = 0.78$ which are the same as the local parameters used for the global DIII-D base case at $r = \frac{1}{2}a$.

Figure 2 shows the ion heat diffusivity χ_i versus R/L_T. Varying R/L_T varies the linear drive of the instability. Note the existence of a nonlinear supercritical region above linear threshold. Similar results have been seen by Dimits and Sydora.[24,27,28] The growth rate shown here was obtained by measuring $|\phi(t)|^2$ in the linear phase of the nonlinear runs.

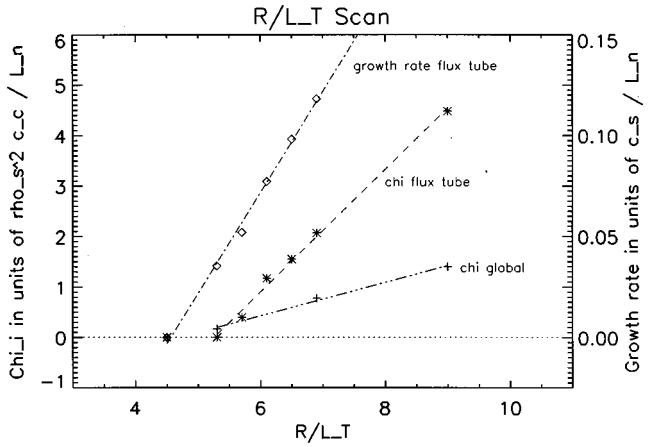

FIG. 2. Ion heat diffusivity, χ_i versus R/L_T for both flux-tube and global simulations. Varying R/L_T varies the linear drive of the instability. Note the existence of a nonlinear subcritical region above linear threshold. Parameters are from the D-IIID Cyclone base case.

III. EFFECTS OF PROFILE VARIATION

There are many nonlocal effects that contribute to the difference between global and flux-tube simulations. These so-called ''nonlocal effects'' simply result from equilibrium quantities varying as a function of minor radius other than first order. As discussed above, flux-tube models typically assume local values for gradients, e.g., $\hat{s}$, L_T, L_n, or equivalently, $q(r-r_0) \approx q(r_0) + (r-r_0)q'(r_0)$, $T_{\rm eq}(r-r_0) \approx T_{\rm eq}(r_0) + (r-r_0)T'_{\rm eq}(r_0)$, etc. All these nonlocal effects contribute to differences between the two models, and are typically linearly stabilizing because, in addition to magnetic shear, these effects cause resonances between the natural frequencies in the local dispersion relation to be localized to one rational surface.

One important nonlocal effect is pressure profile variation. We characterize this as a radially varying L_T and L_n. The effects of profile variation have been known for awhile because sech^2 radial dependence of L_T and L_n have been implemented in both global and flux-tube models.[1,12] However, it is most typical to run a flux-tube code with constant L_T and L_n because this is the most appropriate limit, consistent with the assumptions of the model discussed in Sec. II. More careful comparisons of small global simulations and flux-tube simulations without profile variation using the same local parameters showed order-of-magnitude differences between the two models.[29] Later, we found these differences could be explained by including profile variation in the flux-tube model.[30,31] Similar results using an annular model have been reported more recently.[4]

Figure 3 shows the ion heat diffusivity χ_i versus the profile width w as defined in Sec. II. All these runs were using the DIII-D base case parameters, but with varying profile width. The global simulations where done with a $128 \times 128 \times 64$ grid, 4.2 million particles, and a minor radius of $96\rho_s$. The flux-tube simulations were done with a $64 \times 64 \times 32$ grid and 1 million particles. Figure 3 shows that there is

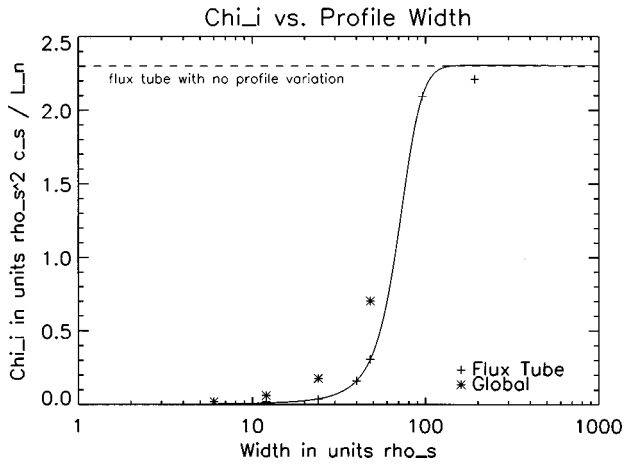

FIG. 3. Ion heat diffusivity, χ_i, versus profile width, w, for both flux-tube and global simulations. Parameters are from the D-IIID Cyclone base case.

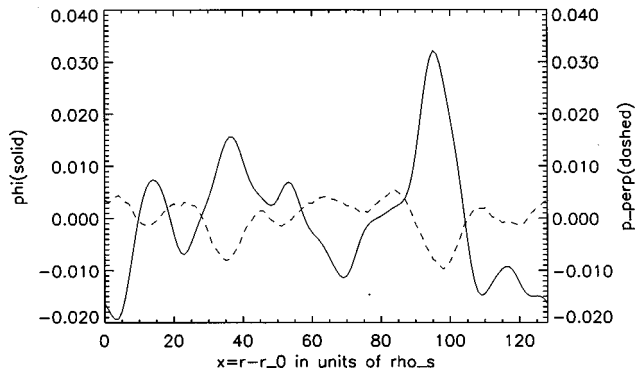

FIG. 5. No profile variation or a profile width of infinity (this is the typical flux-tube limit). Purely radial mode fluctuates. (a) Flux surface average electrostatic potential $\langle\phi\rangle(x)$, and (b) perpendicular ion pressure $\langle P_\perp\rangle(x)$ versus $x=r-r_0$. Parameters are from the D-IIID Cyclone base case.

a fairly sudden transition or drop in the heat flux for the flux-tube simulation around $40-50\rho_i$. This is true qualitatively for the global simulation as well, though larger values of w are not obtainable because strongly unstable local conditions near the boundary violate the assumptions of the model.

Figures 4 and 5 show flux-tube results with $w=12\rho_i$ and $w\to\infty$, respectively. Figure 4, using strong profile variation, shows a localization of the radial mode which is typical of what was first found in small global simulations.[32] Figure 5 shows a more turbulent purely radial mode which is typical of what is found in larger flux-tube simulations.[27,14] In past comparisons of flux-tube and global simulations, global simulations had heat fluxes that were significantly lower (as much as a factor of 20).[29] This qualitative difference can be explained by Fig. 3. Small global simulations done in the past operated in a region below the transition around $40\rho_i$, hence the resulting heat flux was very small. Figure 3 is generated with one set of local parameters and more work is needed to parameterize the critical value of w.

An important observation is that there is a close correlation between $\langle P_\perp\rangle$ and $\langle\phi\rangle$, which seems to be a general result in the flux-tube simulations (see Figs. 4 and 5). In the simulation, it is easier to measure $\langle P_\perp\rangle=\langle\int(v_\perp^2/2)\delta f\, d^3v\rangle$ rather than $\langle T_\perp\rangle$. Simulation results show that $\langle n\rangle\ll\langle T_\perp\rangle$, and this is also shown theoretically below. Therefore, we will assume in our discussion of the results that $\langle T_\perp\rangle\approx\langle P_\perp\rangle$.

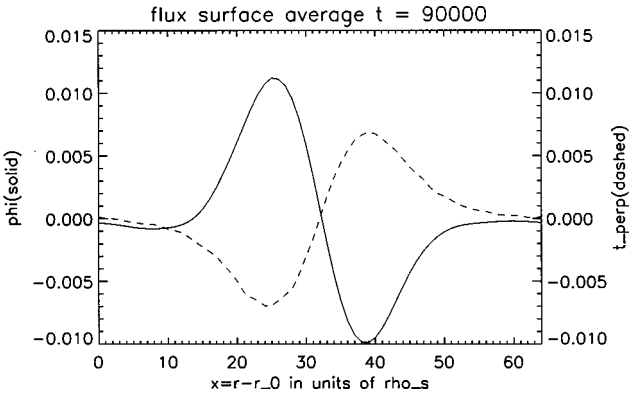

FIG. 4. Strong profile variation with a profile width $w=12\rho_i$. Purely radial mode is stationary. (a) Flux surface average electrostatic potential $\langle\phi\rangle(x)$, and (b) perpendicular ion pressure $\langle P_\perp\rangle(x)$ versus $x=r-r_0$. Parameters are from the D-IIID Cyclone base case.

We can understand the relationship between $\langle T_\perp\rangle$ and $\langle\phi\rangle$ by examining the guiding-center gyrofluid equations for the purely radial modes. The quasi-neutrality condition (or gyrokinetic Poisson equation) for small $k_\perp^2\rho_i^2$ is[33]

$$-\nabla_\perp^2\phi+\frac{1}{\tau}(\phi-\langle\phi\rangle)=\left(1+\frac{1}{2}\nabla_\perp^2\right)n+\frac{1}{2}\nabla_\perp^2 T_\perp, \qquad (10)$$

where $\tau=T_e/T_i$, and $\langle\phi\rangle$ means the flux-surface averaged ϕ. $n=\delta n_i/n_0$ and $T_\perp=\delta T_{\perp,i}/T_{0i}$, and δn_i and $\delta T_{\perp,i}$ are the perturbed guiding-center ion density and temperature, respectively. Perpendicular length scales are normalized to the ion gyro-radius, ρ_i.

For the purely radial modes, this reduces to

$$k_r^2\langle\phi\rangle=(1-\tfrac{1}{2}k_r^2)\langle n\rangle-\tfrac{1}{2}k_r^2\langle T_\perp\rangle. \qquad (11)$$

This equation simply shows that there is a relation between $\langle n\rangle$, $\langle T_\perp\rangle$, and $\langle\phi\rangle$ and not any causality. The gyrofluid equations for $\langle n\rangle$ and $\langle T_\perp\rangle$ in the small $k_\perp^2\rho_i^2$ limit and neglecting toroidal effects are

$$\frac{\partial\langle n\rangle}{\partial t}+\langle\mathbf{v}_E\cdot\nabla n\rangle=0, \qquad (12)$$

$$\frac{\partial\langle T_\perp\rangle}{\partial t}+\langle\mathbf{v}_E\cdot\nabla T_\perp\rangle=0, \qquad (13)$$

where $\mathbf{v}_E$ is the $E\times B$ drift velocity. This simple form is the result of both $k_\parallel$ and k_θ being zero for purely radial modes. Substituting Eq. (10) into Eq. (12) we obtain a Hasegawa–Mima-type[34] equation for the purely radial modes:

$$\frac{\partial}{\partial t}\nabla_r^2\left(\langle\phi\rangle+\frac{\langle T_\perp\rangle}{2}\right)-\left\langle\mathbf{v}_E\cdot\nabla\nabla_\perp^2\left(\phi+\frac{T_\perp}{2}\right)\right\rangle=0. \qquad (14)$$

If we designate integers (l,m,n) to represent the wave numbers (or eigenfunction quantum numbers), i.e., $(k_r,k_\theta,k_\parallel)$, then nonlinear mode coupling of the following form generates purely radial modes

$$(l,m,n)+(l',-m,-n)\rightarrow(l+l',0,0). \tag{15}$$

We assume the generation of purely radial modes primarily involves coupling between the unstable eigenfunctions excited in the stationary turbulence. There may also be couplings between different purely radial modes with different radial eigennumbers. Next, we make two assumptions. First, we assume the contribution from the $T_\perp$ $E\times B$ nonlinearity is larger than the ion polarization nonlinearity in the second term on the left-hand side of Eq. (14). This is reasonable since $T_\perp$ is larger than ϕ from linear theory where $T_{\perp,k}\sim(\omega_{*T}/\omega)\phi_k$. Second, we assume we can write the nonlinear term the following way:

$$\sum_{\mathbf{k}=\mathbf{k}'+\mathbf{k}''}\hat{\mathbf{b}}\times\mathbf{k}'\cdot\mathbf{k}''k''^2_\perp\phi_{\mathbf{k}'}T_{\perp,\mathbf{k}''}$$

$$\approx\overline{k^2_\perp}\sum_{\mathbf{k}=\mathbf{k}'+\mathbf{k}''}\hat{\mathbf{b}}\times\mathbf{k}'\cdot\mathbf{k}''\phi_{\mathbf{k}'}T_{\perp,\mathbf{k}''}, \tag{16}$$

where $\overline{k_\perp}$ is representative of the background turbulent fluctuations which drive the (0,0) modes. Using these assumptions along with Eqs. (13) and (14), we can solve for $\langle\phi\rangle$ in terms of $\langle T_\perp\rangle$ to obtain the following important result:

$$\langle\phi\rangle\approx-\frac{1}{2}\left(1+\frac{\overline{k^2_\perp}}{k^2_r}\right)\langle T_\perp\rangle, \tag{17}$$

where k_r is the radial wave number of $\langle\phi\rangle$. To summarize, the equation governing the flux-surface-averaged ion polarization density turns out to be very similar to the equation governing the flux-surface-averaged perpendicular ion temperature. This makes the problem solvable.

Equation (17) explains the stationary, almost sinusoidal shape of the purely radial modes in the situation where there is strong profile variation, Fig. 4. The heat flux attempts to flatten the temperature profile generating a $\langle T_\perp\rangle$ as shown in Fig. 4. This nonlinearly generates $\langle\phi\rangle$ from Eq. (17). For the case with no profile variation, or constant L_T, the fluctuations in $\langle T_\perp\rangle$ coming from fluctuations in the heat flux are turbulent as expected, as seen in Fig. 5. Although this explanation of the generation of $\langle\phi\rangle$ appears complete, it is important to realize that past simulations have shown that there is radial mode generation even in the absence of FLR effects.[32,35] However, even in the absence of FLR effects, there will be drift orbit averaging that may lead to a similar effect. Also, note that this effect is *not* simply the balancing of E_r and ∇P in the radial force balance equation, but is a nonlinear generation of $\langle n\rangle$, which in turn generates E_r.

IV. TRANSPORT REDUCTION USING PROFILE RIPPLE

As shown in Sec. III, a flux-surface-averaged perpendicular ion temperature perturbation can nonlinearly drive a purely radial electric field. It may be possible to add a slight ripple ($\sim$5%) or small bumps to the equilibrium temperature profile on the scale of $\sim 30\rho_i$ to enhance the self-generated shear flows and thereby reduce turbulent transport. For example, say the equilibrium temperature profile had the following form:

$$T_{\mathrm{eq}}(r)=T_0(r)[1+\epsilon\cos(k_0x)]. \tag{18}$$

Then, the corresponding temperature gradient or drive of the instability would be

$$L_T^{-1}=-\frac{1}{T}\frac{dT}{dr}\approx\frac{-1}{T_0}\frac{dT_0}{dr}\epsilon k_0\sin(k_0x) \tag{19}$$

$$=L_{T0}^{-1}[1+\epsilon k_0L_{T0}\sin(k_0x)]. \tag{20}$$

Hence, very modest short-scale ripple of the temperature profile causes much larger variations in L_T for $L_Tk_0\gg1$. This variation of the drive causes stationary spatial oscillations in $\langle T_\perp\rangle(x)$, which in turn nonlinearly generates E_r shear, that then suppresses the turbulent transport. Figure 6 shows $\langle\phi\rangle$ and $\langle P_\perp\rangle$ from a flux-tube simulation with a 34% variation in L_T^{-1}, which corresponds to only a 2% temperature ripple. For this case, using typical H-mode (high confinement mode) parameters, there was a 60% reduction in the ion heat flux.

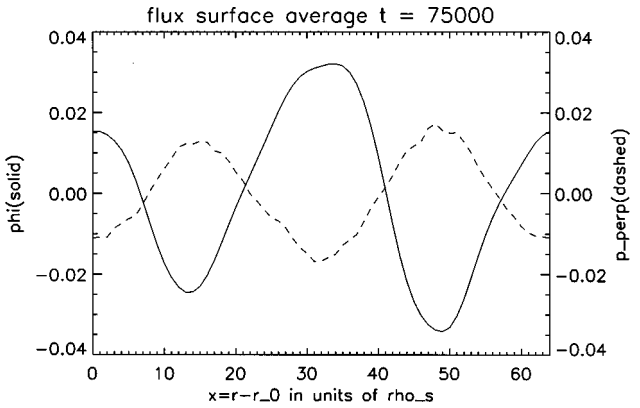

FIG. 6. Weak, short-scale sinusoidal variation of the temperature profile reduces the heat flux by 60%. $T_{\mathrm{eq}}(r)\approx T_0(r)(1+0.02\cos(0.2r/\rho_i))$ (a) Flux-surface average electrostatic potential $\langle\phi\rangle(x)$, and (b) perpendicular ion pressure $\langle P_\perp\rangle(x)$ versus $x=r-r_0$. Parameters are from the D-IIID Cyclone base case.

It is important to realize that equilibrium E_r shear[36–40] is *not* included in the test simulation of Fig. 6. The radial force balance is

$$E_r=\frac{1}{en_i}\frac{dP_i}{dr}+u_\phi B_\theta-u_\theta B_\phi. \tag{21}$$

Therefore, the ripple in the temperature may cause a ripple in the equilibrium E_r. Assuming, there is no fluid flow, there will be a ripple in the equilibrium potential from the temperature ripple and from Eq. (21), $\delta\phi_{\mathrm{eq}}=-\delta T_{\mathrm{eq}}$. Hence, the nonlinearly generated $\langle\phi\rangle$ from Eq. (17) may cancel the equilibrium E_r. We may be able to choose parameters such that $k_r^2\ll\overline{k_\perp^2}$ which would cause the self-generated E_r shear to dominate. More work is needed to carefully parametrize the relationship between equilibrium and self-generated E_r shear when the temperature profile is rippled to avoid cancellation between the two. Another practical issue is how to actually generate a small and relatively short-scale temperature pro-

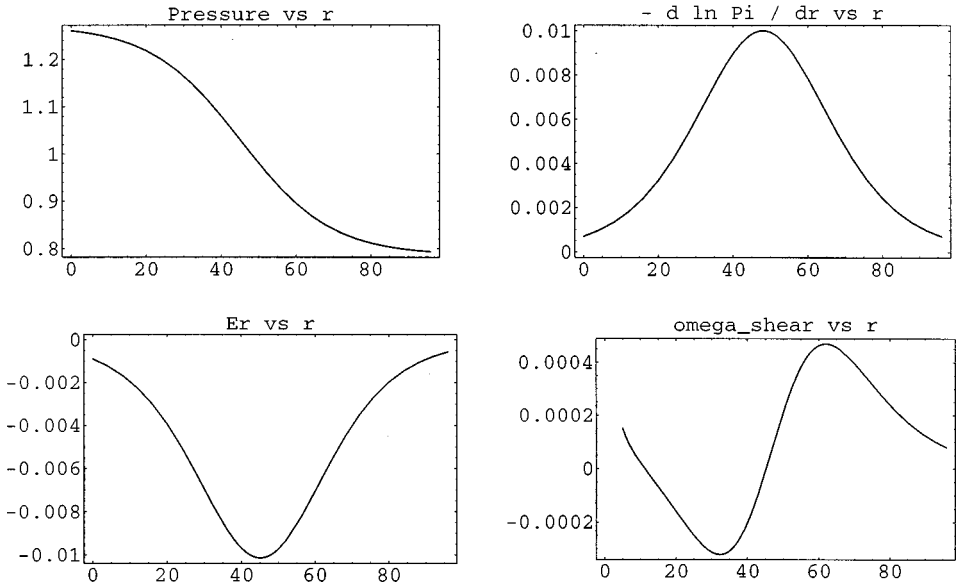

FIG. 7. Profiles used for studying the effects of equilibrium E_r shear. (a) Temperature profile, (b) $1/L_T(r) = -[1/T(r)][dT(r)/dr]$, (c) equilibrium E_r from radial force balance Eq. (21), and (d) shearing rate, $\omega_s h(r)$. The parameters are discussed further in the text.

file variation from flux surface to flux surface. This may be possible using ion-cyclotron resonance heating with multiple rf (radio frequency) sources or variable frequency. This would rely on some focusing of the launched wave toward the the vertical center of the plasma. Not restricting our discussion to present-day rf systems, one plausible scheme would be to frequency modulate the rf heating carrier frequency with a staircase waveform, causing a slight heating of flux-surfaces spaced $\sim 30\rho_i$ apart.

V. EQUILIBRIUM E_R SHEAR FROM PROFILE VARIATION

Section III included the turbulent self-generated shear flows, as well as the so-called ''variation in ω_*'' effects. Our discussion so far *did not* include equilibrium E_r shear coming from radial force balance, Eq. (21). To briefly show the additional effect of equilibrium E_r, we assume $n_i(r)$, $T_i(r)$, and the toroidal rotation, $\Omega_\phi(r)$, are given equilibrium quantities (inputs to the simulation). The toroidal flow is given by $u_\phi = \Omega_\phi(r)R$. Equilibrium poloidal flow is neglected, assuming it will be neoclassically damped[41] to small values. However, the self-generated purely radial $E\times B$ flows (or zonal flows) are fully taken into account here and throughout the paper. Assuming $u_E \ll v_{ti}$ the gyrokinetic equations of motion are[42]

$$\dot{\mathbf{R}} = v_\parallel \hat{\mathbf{b}} + \frac{c}{B}\left[\hat{\mathbf{b}}\times(\nabla\delta\phi - E_r\hat{r}) + \frac{\mu}{e}\hat{\mathbf{b}}\times\nabla B + \frac{m_i}{e}v_\parallel^2\hat{\mathbf{b}}\times\hat{\mathbf{b}}\cdot\nabla\hat{\mathbf{b}}\right], \tag{22}$$

$$\dot{v}_\parallel = -\left[\hat{\mathbf{b}} + \frac{m_i}{eB}v_\parallel\hat{\mathbf{b}}\times\hat{\mathbf{b}}\cdot\nabla\hat{\mathbf{b}}\right]\cdot\left[\frac{e}{m_i}(\nabla\delta\phi - E_r\hat{r}) + \frac{\mu}{m_i}\nabla B\right]. \tag{23}$$

We also take the simplest analytic equilibrium with $T_\parallel = T_\perp$:

$$f_0(v_\parallel,\mu) = n_0\left(\frac{m_i}{2\pi T_i}\right)^{3/2}\exp\left[-\frac{\mu B}{T_i} - \frac{m_i}{2T_i}(v_\parallel - u_\phi)^2\right]. \tag{24}$$

Figure 7 shows typical profiles used to study the effect of equilibrium E_r shear. In this case $1/L_n = 0$, and $u_\phi = 0$. Figure 7(a) (upper left) shows the ion temperature profile and Fig. 7(b) (upper right) shows $1/L_T(r)$. Figure 7(c) (lower left) shows the resulting $E_r(r)$, and Fig. 7(d) (lower-right) the $E\times B$ shearing rate $\omega_s = (RB_\theta/B)(d/dr)(E_r/RB_\theta)$, where ω_s can be compared with the linear growth rate or the decorrelation time of the turbulence for determining turbulent transport suppression.[36–40] Figure 8 shows χ_i versus the profile width w for cases with and without equilibrium E_r from radial force balance Eq. (21). Using the definitions of Sec. II, the parameters are: 4 million particles, a $128\times128\times64$ grid, $\Delta x = \Delta y = 1.5\rho_s$, $\Delta t c_s/L_T = 0.2$. The physical pa-

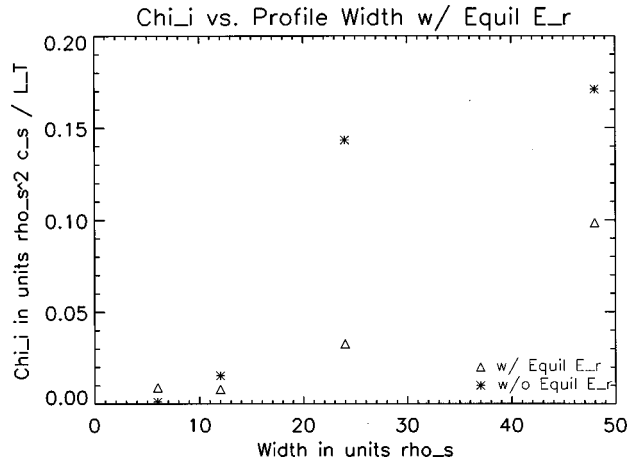

FIG. 8. Ion heat diffusivity, χ_i, as a function of profile width. The asterisk data points are without equilibrium E_r shear, and the diamond data points are with the equilibrium E_r shear. The equilibrium E_r shear is an additional stabilizing effect and changes the character of the transition to stability (more gradual). Self-generated E_r is included in both cases. The parameters are discussed in the text.

rameters are $R_0/L_T(r_0)=6.96$, $R/L_n(r_0)=\infty$, $T_i=T_e$, $a=96\rho_s$, and $R_0=696\rho_s$, $q_0=1.25$, $\Delta q=3.0$, $r_0=\frac{1}{2}a$, and $q(r_0)=2.0$. Figure 8 shows that the equilibrium E_r is stabilizing, as expected. One noticeable difference with equilibrium E_r is that the sudden transition to low values of heat flux as w is reduced is replaced by a more gradual linear shutoff. More work is needed to characterize the effects with equilibrium shear flow coming from profile variation versus toroidal shear flow. Waltz[43] and Dimits[2] have characterized the effects of equilibrium E_r shear flow, but not the combined effect of E_r shear and variation of ω_* as shown here.

VI. SUMMARY

Large-scale gyrokinetic simulations are now much more realistic than past particle or Vlasov turbulence simulations. The current challenge is not simply to compare with experiment, but also to show a reasonable consistency between the various simulation models currently in use and to understand why the differences exist. Two common computational domains used are a global volume (or whole cross section), and a flux-tube volume (using radially local parameters). Past comparisons have shown large differences[29] between these two models. Here, we discuss equilibrium profile variation which is one of the primary differences between the two models. Profile variation in a flux-tube model was compared with global results with the same parameters. It was found that as the profile width is varied from large to small values, there is a fairly sudden transition to very low values of ion heat flux. This may explain the low heat flux values from past small global simulations. In addition, strong profile variation causes a stationary ''global'' radial mode as seen previously.[32]

It was shown that the behavior of the purely radial mode can be predicted from the perpendicular flux-surface-averaged ion temperature. With significant profile variation, the heat flux flattens the equilibrium temperature, leading to the generation of the global purely radial mode. On the other hand, when the temperature gradient is constant, there is no preferred location of profile flattening and the radial mode is then more turbulent, which is what is observed in constant L_T flux-tube simulations. The profile variation also causes an equilibrium E_r shear through radial force balance. This effect was included and shown to be further stabilizing.

The fact that the self-generated E_r is closely related to $\langle T_\perp \rangle$ leads to a possible method to reduce ion heat transport. If the temperature profile can be rippled on a scale of $\sim 30\rho_i$ using ion-cyclotron resonance heating or some other mechanism, the associated rippled heat flux and $\langle T_\perp \rangle$ may result in significant E_r shear. The combined effects of equilibrium and self-generated shear with temperature profile ripple need to be explored further to ensure cancellation of the two effects can be avoided. It was shown in gyrokinetic simulations of ITG turbulence that very weak (2%), short-scale ripple in the equilibrium temperature profile can reduce the ion heat flux by more than a factor of 2.

ACKNOWLEDGMENTS

We especially thank all the members of the ''Cyclone Team,'' including Dr. M. Beer, Dr. C. Bolton, Dr. B. Cohen, Dr. A. Dimits, Dr. W. Dorland, Dr. G. Hammett, Dr. W. Nevins, Dr. D. Shumaker, and Dr. R. Sydora. We are also grateful to Dr. V. Decyk, Dr. T. S. Hahm, Dr. R. Majeski, Dr. F. Perkins, and Dr. T. Tran for their help and input. This research is supported by U.S. Department of Energy (DOE) Grant No. DE-FG03-97ER5442(4/6). This work is an active part of the Numerical Tokamak Turbulence Project DOE Grand Challenge. Computing resources where generously provided by the Advanced Computing Laboratory at Los Alamos National Laboratory and the National Energy Research Scientific Computing Center at Lawrence Berkeley National Laboratory.

[1] S. Parker, W. Lee, and R. Santoro, Phys. Rev. Lett. **71**, 2042 (1993).
[2] A. Dimits, T. Williams, J. Byers, and B. Cohen, Phys. Rev. Lett. **77**, 71 (1996).
[3] R. Sydora, V. Decyk, and J. Dawson, Plasma Phys. Controlled Fusion **38**, A281 (1996).
[4] Z. Lin, T. Hahm, W. Lee, W. Tang, and R. White, Science **281**, 1835 (1998).
[5] E. Frieman and L. Chen, Phys. Fluids **25**, 502 (1982).
[6] W. Lee, Phys. Fluids **26**, 556 (1983).
[7] A. Dimits and W. Lee, J. Comput. Phys. **107**, 309 (1993).
[8] S. Parker and W. Lee, Phys. Fluids B **5**, 77 (1993).
[9] G. Hu and J. Krommes, Phys. Plasmas **1**, 863 (1994).
[10] S. Parker, H. Mynick, M. Artun, V. Decyk, J. Kepner, W. Lee, and W. Tang, Phys. Plasmas **3**, 1959 (1996).
[11] J. Kepner, S. Parker, and V. Decyk, SIAM News **30**, 1 (1997).
[12] S. Parker, W. Dorland, R. Santoro, M. Beer, Q. Liu, W. Lee, and G. Hammett, Phys. Plasmas **1**, 1461 (1994).
[13] S. Parker, M. Artun, V. Decyk, J. Kepner, W. Lee, H. Mynick, and W. Tang, in *Advanced Series in Nonlinear Dynamics, Vol. 9*, edited by S. Benkadda, F. Doveil and Y. Elskens (World Scientific, Singapore, 1996).
[14] M. Beer, S. Cowley, and G. Hammett, Phys. Plasmas **2**, 2687 (1995).
[15] B. Cohen, in *Multiple Time Scales*, edited by J. U. Brackbill and B. I. Cohen, (Academic, New York, 1985).
[16] D. Dubin, J. Krommes, C. Oberman, and W. Lee, Phys. Fluids **26**, 3524 (1983).
[17] T. S. Hahm, Phys. Fluids **31**, 2670 (1988).
[18] A. J. Brizard, J. Plasma Phys. **41**, 541 (1989).
[19] This list of papers may not be complete and includes only the later work on nonlinear gyrokinetics. Please check references within.
[20] W. Dorland and G. Hammett, Phys. Fluids B **5**, 812 (1993).
[21] W. W. Lee, J. Comput. Phys. **72**, 243 (1987).
[22] M. LeBrun, T. Tajima, M. Gray, G. Furnish, and W. Horton, Phys. Fluids B **5**, 752 (1993).
[23] E. Strait, L. Lao, M. Mauel, B. Rice, T. Taylor, K. Burrell, M. Chu, E. Lazarus, T. Osborne, S. Thompson, and A. Turnbull, Phys. Rev. Lett. **75**, 4421 (1995).
[24] ''U.S. Contributions to ITER Urgent R & D on *H*-mode Core Confinement,'' S. D. Scott and M. C. Zarnstorff, Oct. 16, 1997; A. M. Dimits *et al.*, to be submitted to Phys. Plasmas.
[25] S. Cowley, R. Kulsrud, and R. Sudan, Phys. Fluids B **13**, 2767 (1991).
[26] R. B. White and M. S. Chance, Phys. Fluids **27**, 2455 (1984).
[27] A. Dimits, B. Cohen, N. Mattor, W. Nevins, D. Shumaker, S. Parker, and C. Kim, UC-LLNL report: UCRL-JC-130166; Paper IAEA-F1-CN-69/TH1/1, to appear in the proceedings of the 17th IAEA Fusion Energy Conference, 19–24, 19–24 October 1998, Yokohama, Japan (International Atomic Energy Agency, Vienna, 1998).
[28] This effect was first seen in the Cyclone Team comparisons by A. M. Dimits and R. D. Sydora.
[29] S. Parker, T. Hahm, and W. Lee (private communication, 1997).
[30] C. Kim and S. E. Parker, Bull. Am. Phys. Soc. **42**, 1986 (1997).
[31] C. Kim and S. E. Parker (private communication, 1998).
[32] J. C. Cummings, Ph.D. thesis, Princeton University, 1994.

[33]W. Dorland, Ph.D. thesis, Princeton University, 1993.
[34]A. Hasegawa and K. Mima, Phys. Fluids **12**, 87 (1983).
[35]B. Cohen, A. Dimits, T. Williams, and J. Byers, Phys. Fluids B **5**, 2967 (1993).
[36]H. Biglari, P. Diamond, and P. Terry, Phys. Fluids B **2**, 1 (1990).
[37]P. Diamond and Y. Kim, Phys. Fluids B **3**, 1626 (1991).
[38]S. Hamaguchi and W. Horton, Phys. Fluids B **4**, 319 (1992).
[39]T. Hahm and K. H. Burrell, Phys. Plasmas **2**, 1648 (1995).
[40]R. Waltz, G. Kerbel, and J. Milovich, Phys. Plasmas **1**, 2229 (1994).
[41]T. H. Stix, Phys. Fluids B **16**, 1260 (1973).
[42]T. S. Hahm, Phys. Plasmas **3**, 4658 (1996).
[43]R. Waltz, R. Dewar, and X. Garbet, Phys. Plasmas **5**, 1784 (1998).